Composite Structures 160 (2017) 195–203

Contents lists available at ScienceDirect

Composite Structures

journal homepage: www.elsevier.com/locate/compstruct

Non-destructive characterization of fiber orientation in reinforced SMC as input for simulation based design

Katja Schladitz [a,*], Andreas Büter [b], Michael Godehardt [a], Oliver Wirjadi [a], Johanna Fleckenstein [b], Tobias Gerster [c], Ulf Hassler [d], Katrin Jaschek [b], Michael Maisl [e], Ute Maisl [e], Stefan Mohr [d], Udo Netzelmann [e], Tobias Potyra [f], Martin O. Steinhauser [c,g]

[a] Fraunhofer ITWM, Fraunhofer-Platz 1, 67663 Kaiserslautern, Germany
[b] Fraunhofer LBF, Bartningstrasse 47, 64289 Darmstadt, Germany
[c] Fraunhofer EMI, Eckerstrasse 4, 79104 Freiburg, Germany
[d] Fraunhofer IIS, Am Wolfsmantel 33, 91058 Erlangen, Germany
[e] Fraunhofer IZFP, Campus E3.1, 66123 Saarbrücken, Germany
[f] Fraunhofer ICT, Joseph-von-Fraunhofer-Strasse7, 76327 Pfinztal, Germany
[g] Dept. of Chemistry, University of Basel, Klingelbergstr. 80, 4056 Basel, Switzerland

ARTICLE INFO

Article history:
Received 4 April 2016
Revised 7 October 2016
Accepted 8 October 2016
Available online 13 October 2016

Keywords:
B Mechanical properties
C Anisotropy
D Non-destructive testing
Quantitative image analysis

ABSTRACT

The macroscopic properties of materials are strongly influenced by their microstructure. This holds in particular for fiber reinforced composites where fiber distribution and orientation are crucial for the reinforcement to serve its purpose. This essential microstructural information can be obtained from high-resolution images using appropriate methods for quantitative image analysis. Sheet molding compounds feature a very dense layered system of reinforcing fibers and a particularly strong X-ray absorption. Therefore, in this case, state-of-the-art fiber orientation analysis based on 3D images obtained by X-ray microtomography faces problems. In this paper, we determine the local fiber orientation in each pixel by the orientation of the anisotropic Gaussian filter yielding the strongest filter response. Hence, the local fiber orientation can be computed without identifying individual fibers. From the thus determined area weighted orientation distribution, the degree of anisotropy and the main fiber orientation are derived. This extremely robust analysis method is applied to 2D slice images from scanning acoustic microscopy and high-resolution 3D microtomography. We show that the Gaussian filter based fiber orientation analysis method yields comparable results for both imaging techniques. Moreover, comparison with fatigue tests performed on the same specimens proves the image analytically determined fiber orientation and the failure behaviour to be strongly correlated. In particular, a critical degree of anisotropy could be identified. For degrees of anisotropy higher than this limit, the samples behave mechanically like a uniaxial material. The paper thus provides experimentally validated evidence for calibrating micro-mechanical models for subsequent simulation of macroscopic material properties using the combination of high-resolution imaging techniques and quantitative image analysis.

1. Introduction

The mixing of fibers and polymers to form composites opens new ways for designing lightweight materials substituting traditionally used steel alloys or iron sheets in aviation and car industry [1]. Composite materials are traditionally regarded as materials that can save energy in large structures and components associated with transportation. Some of the most interesting applications of fiber reinforced composite materials are those where they are used to protect lives or property by absorbing energy in impacts or crashes [2,3].

Impact is considered as one of the most dangerous damage sources of fiber reinforced polymeric composite structures, as it can lead to significant reduction on the strength and stiffness of the structures. However, the damage can often not be detected from mere surface inspection of the component, thus causing great security risks to the structures.

* Corresponding author.
E-mail address: katja.schladitz@itwm.fraunhofer.de (K. Schladitz).
URL: http://www.itwm.fraunhofer.de (K. Schladitz).

http://dx.doi.org/10.1016/j.compstruct.2016.10.019
0263-8223/

Among various composite systems, the sheet molding compounds (SMCs) have been increasingly used for structural applications because of their excellent processibility and versatility in manufacture and desirable mechanical properties for engineering design. SMCs are high strength glass or carbon reinforced thermoset molding materials processed by thermocompression. SMC composites combine glass or carbon fiber and unsaturated polyester/vinylester modified resins to produce a high-strength molding compound [4,5].

The rapid increase in applications of short- and long-fiber reinforced SMCs as safety-relevant parts and components has resulted in significant concern over the failure behavior of the material. In this context, many experimental studies have been performed to measure the mechanical response of SMCs to a variety of loading conditions such as crash impact [6–8], fluctuating temperature environments [9,10] or different strain rates [11,12]. While such experiments provide data for a useful analytic description of the studied material behavior and for deriving constitutive equations that can be used in numerical studies, they do not provide any detailed microstructural information about fiber orientation in different layers of the SMC material.

Recently, with the rapid development of computer speed and computational methods, such as the Discrete Element Method (DEM) and the Finite Element Method (FEM), numerical simulations on multiscales, taking into account different structural features of materials not only on the macroscopic, but also on the microscopic scale, have become feasible [13–16]. Thus, for numerical simulations, a better understanding of the connection between the spatial distribution of microscopic fibers, controlling the macroscopic performance, has become a major issue.

Knowing the composition of the precursors as well as the production process of fiber reinforced composites provides broad qualitative information about the microstructure, for instance fiber volume fraction, preferred fiber direction or layers within the microstructure. However, quantitative image analysis is needed in order to go beyond mere qualitative descriptions of composite materials and to obtain detailed local microstructural information that can be used as input for numerical simulation tools [17]. In particular, local deviations from the expected fiber content or direction have to be taken into account when designing parts. Also, enhanced virtual component design before manufacturing a single part requires quantitative image analysis: The software packages for computer aided design need as input not only the material properties of the components but also microstructural features that have to be acquired image analytically.

Traditional approaches in materialography are based on light-microscopic 2D images of microsections and provide measurements of fiber volume fraction and its local variation. There exists a variety of methods for the so-called binarization, i.e., the separation of an image into foreground (fibers) and background areas [18,19]. Anisotropy can be quantified using linear contact or chord length distributions [20]. 3D fiber directions can be estimated from 2D microsections using the elliptical shape of fiber cross-sections [21,22]. However, this approach requires individual fibers to be segmented, i. e. identified as individual objects within the image, and that the resolution is high enough to reliably measure the cross-sectional shape. Fiber directions in fiber reinforced SMC have been studied as early as 1986 using the high X-ray absorption contrast of lead doped glass fibers in radiographs [23]. Advani provides a comprehensive overview of early orientation analysis methods [24]. Confocal laser scanning microscopy allows to image layers up to a depth of about 30 μm and was used to decrease the error in orientation measurements based on the shape of elliptical cross-sections [25,26].

In SMC composites, bundles formed of long fibers have to be analyzed. Thus methods thriving on the segmentation of individual fibers are not applicable and approaches for determining local fiber directions without segmentation of individual fibers have to be considered. Le et al. [5] segmented individual bundles manually exploiting high lateral and gray value resolutions achieved by synchrotron radiation computed tomography. The so-called chord length transform and the method based on axis and moments of inertia thrive on ideas from mathematical morphology [27,28]. A refinement of the latter method has been used by Viguié et al. [29] to segment and individually analyze fiber bundles in an SMC sample imaged by micro computed tomography (μCT). Krause et al. deduced local directions from first order derivatives (gradients) subsumed in the structure tensor [30]. The Hessian matrix of second partial derivatives yields the local fiber direction as the direction corresponding to its lowest eigenvalue [31,32].

In this paper, scanning acoustic microscopy (SAM) and μCT are combined with a local orientation analysis method based on anisotropic Gaussian filters [33,34,32] since this method is particularly well suited for large, rather roughly resolved images of fiber reinforced SMC. This paper introduces this method for the first time in an application setting, shows its robustness, and its applicability to images from very different sources. In particular, analysis results based on SAM and μCT are found to be comparable.

The method based on anisotropic Gaussian filters is particularly well-suited for the SMC samples considered here as it

(a) allows to extract the local fiber orientation information without error-prone and tedious segmentation of individual fibers or fiber bundles,
(b) is robust with respect to noise [32] and not well defined edges, and
(c) can be computed very efficiently for orientation distributions concentrated in a plane [34].

From the local fiber orientation distribution, a measure for anisotropy is deduced, which can be directly correlated with the observed fatigue strength of the specimens thus experimentally confirming rules of thumb on the relation of the degree to which the fibers are oriented and mechanical behaviour.

The organization of the paper is as follows: A short description of the material studied is followed by a summary of the imaging techniques used. Subsequently, we describe the measurement of fiber orientation in the material samples and the fatigue tests. The agreement of the experimental results – image analytically determined fiber orientation and cumulative fatigue strength – is emphasized in a dedicated section just before the final conclusions.

2. Material and methods

2.1. Sheet molding compounds

Essentially, there are two strategies for assembling a composite – stacking layers of different materials yielding a laminate or inserting particles into a matrix to get a particle reinforced composite. Fiber reinforced SMC falls into the first class as it is produced by compression molding. Industrially, SMC is processed in three steps: First, liquid and solid raw materials as unsaturated cross-linked polyesters, thermoplastic processing aids, resin, and mineral fillers are mixed to form a homogeneous resin-filler paste. Reinforcement fibers are incorporated, resulting in a semi-finished SMC panel exhibiting a rather low viscosity which allows the fibers to be effectively wetted with a coating film. Second, the SMC is stored for a while to give the paste time to thicken, or mature. During this process the SMC cures, resulting in an increase of the dynamic viscosity. Finally, the semi-finished SMC panel is formed into a component. The SMC starts to flow due to the pressure,

eventually filling the cavities of the mold and at the same time dragging along the fibers in the resulting flow field. The prediction of the fiber orientation in compression molding is rather difficult. Usually, methods based on the classical model of Jeffery [35] for the motion of short rigid fibers in dilute suspensions assuming a spatially homogeneous flow field are used and extended in several ways to more realistic non–homogeneous situations.

The SMC samples investigated here were produced by depositing the fibers covered by a sizing agent into the fluid resin mixture. Within the deposit range, the fibers are roughly isotropically oriented within the sheet plane. Further away however, fibers are more and more oriented by the flow. The specimens used in the following were cut out of SMC plates by a water jet, an example is shown in Fig. 1(b). Samples were taken far enough from the deposit range that a strong degree of anisotropy can be expected and cut within flow direction, at 45° to the flow direction, and perpendicular to the flow direction.

The target fiber length was 25 mm throughout, whereas varying fiber weight (wt) contents were considered (20%, 30%, and 50%). In the following, fatigue test specimen of the dimensions shown in Fig. 1(b) are used for orientation analysis based on SAM and CT image data, as well as for the quantitative comparison of orientation analysis results and orientation analysis and mechnical testing.

2.2. Scanning acoustic microscopy (SAM)

Acoustic microscopy is a non-destructive imaging technique using high-frequency ultra sound (10 MHz to 2 GHz). The corresponding acoustic wavelengths are clearly in the sub-millimeter range in all materials and thus allow for a microscopic lateral resolution. More precisely, spatial resolutions between 50 and 200 µm can be achieved, depending on the frequency applied and the scattering properties of the investigated material.

Due to the surface quality and the strong total acoustic attenuation of the investigated fiber reinforced SMC specimens, equipment, and transducers in the frequency regime 10–100 MHz were used. Acoustic attenuation is notable, but still small enough to allow penetration depths of several millimeters.

Our experimental setup has originally been developed and successfully applied for detection of small defects in ceramics [36]. It consists of a large water immersion tank with a mechanical scanner with a step resolution of down to 7.5 µm [37,38]. The acoustic

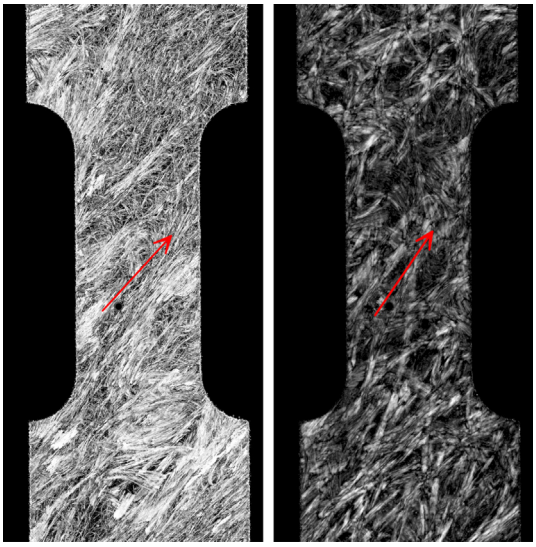

(a) Depth 0.1 mm (b) Depth 0.5 mm

Fig. 2. SAM images from different depths of an SMC fatigue test specimen with 30 wt% fibers. Image analytically measured preferred fiber bundle orientations indicated by red arrows.

damping in water generally reduces the effective frequency range. Due to the ratio of focal length to aperture which usually lies between 3 and 9, and the comparably low sound velocity of a typical SMC (2400 m/s compared to e.g. 12,000 m/s in typical ceramics), the acoustic beam waist is quite large, allowing to select the detection depth just by shifting the time gate.

Fig. 2(a) and (b) exhibit material layers at approximate detection depths 0.1 mm and 0.5 mm, respectively, of a test specimen using high-frequency ultra sound with a nominal frequency of 50 MHz. The structural information is averaged over a slice thickness of 102 μm.

2.3. Micro-computed tomography

A computed tomography (CT) scanner of Fraunhofer EZRT equipped with a Viscom XT 9225-D micro-focus X-ray tube and a Perkin Elmer XRD 1620 AN 1 flat-panel detector with

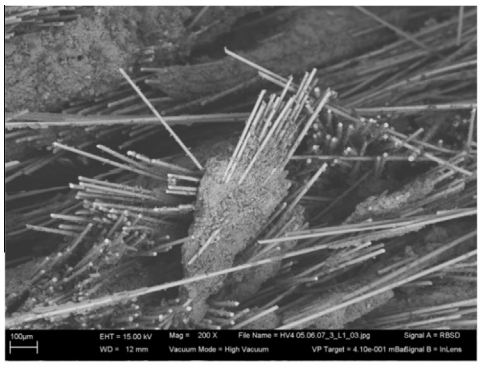

(a) SEM image of a fracture area of an SMC sample depicting glass fiber bundles and the surrounding matrix material

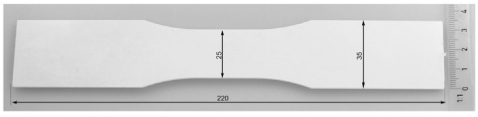

(b) Unnotched flat SMC specimen as used in the measurements and fatigue limit experiments described in the following.

Fig. 1. Material analyzed and tested.

2048 × 2048 pixels allowing high resolution helical CT scans was used. Helical CT is an acquisition geometry originally developed for medical CT and known in this area as spiral scan CT [39]. It was adapted and extended for the application in industrial CT scanners by using dedicated filtering and weighting of the 2D projection images.

The helical acquisition geometry differs from conventional axial CT in the fact that the specimen is moved along the vertical z-direction in each angle step resulting in a helical trajectory. Helical CT is particularly well suited for scanning long objects which require concatenation of the reconstructions from several partial scans when relying to conventional axial CT. In contrast to this, the object can be scanned at once and no further data treatment is necessary when using helical CT. Beam-hardening artifacts were reduced by the iterative artifact reduction method [40].

Fig. 5(d) shows a 2D slice from a CT image of an SMC sample with pixel size 17.3 μm. The CT image data being reconstructed on an isotropic lattice, the slice thickness is 17.3 μm, too.

2.4. Image analytic direction analysis using anisotropic Gaussian filters

Here, we used a different and very robust method, suitable for 2D and 3D images. The core of this method is the computation of local fiber directions based on filtering with anisotropic Gaussians. From this local directional information, the principal direction of fiber alignment, the degree of anisotropy, as well as the orientation tensor can be analytically deduced.

The glass fiber component of fiber reinforced materials can be mathematically modeled as an anisotropic random fiber system Φ in 3D Euclidean space [19]. Let $\subset S^2_+$ denote the upper half-sphere that can be identified with the set of non-oriented directions. The direction distribution we are interested in is defined by the probability measure

$$\rho(A) = \frac{1}{2\pi\,\mathbb{E}\mathrm{vol}(W\cap\Phi)}\mathbb{E}\left(\int_{W\cap\Phi}\mathbf{1}_A[v(x)dx]\right), \tag{1}$$

where $A \subset S^2_+$ is a measurable set of non-oriented directions and the expectations are taken with respect to the distribution of the random fiber system Φ. W denotes the observation window and $v(x) \in S^2_+$ is the direction of the fiber in point x. The volume is denoted by vol and expectation by $\mathbb{E}$. The functional $\mathbf{1}_A$ is the indicator of the set A. That is, $\mathbf{1}_A[v(x)] = 1$ if $v \in A$ and $\mathbf{1}_A[v(x)] = 0$ otherwise. The expectation value is taken with respect to the random fiber system Φ. The fiber direction distribution can be estimated from the lengths of generalized projections onto linear subspaces or from the numbers of intersections with planar subspaces [19,41].

Consider the convolution $(G_v * F)$ of the gray value image F with a Gaussian filter G_v having an elliptical filter mask with long axis $10r$, residual axis $2r$, and direction v of the longer axis. Here, r is set to a rough estimate of the fiber radius. If the pixel x lies within a fiber with local direction μ, then the filter response $(G_v * F)(x)$ should be maximal exactly if $v = \mu$. In other words, the local fiber direction $\widetilde{v}(x)$ in x can be calculated as the direction inducing the strongest filter response

$$\widetilde{v}(x) = \max_v[(G_v * F)(x)], \tag{2}$$

where $\max_v$ denotes the direction maximizing the filter response. See Figs. 4 and 5 for results.

Obviously, Eq. (2) can be used only if v runs through a finite set of directions, covering the space of directions as evenly as possible. In 2D, this is easily achieved using the directions $\pi k/n$ with $k = 1, 2, \ldots, n$ and $n \in \mathbb{N}$, while in 3D the discretization of the orientation space is much more difficult, see e.g. [33,42].

An efficient implementation of the filtering procedure with anisotropic Gaussian filters is essential and can be achieved following the approach proposed by Lampert and Wirjadi [34] which is based on the same concepts as the separability of isotropic Gaussian filters. Separability there means that the n-dimensional convolution integral can be implemented as a sequence of n one-dimensional convolutions along the coordinate axes. However, for general anisotropic Gaussians, separability is not immediately at hand. Nevertheless, by implementing an intuitive, geometrically motivated separation scheme, one can achieve faster anisotropic Gaussian filtering than is possible with commonly used methods based on the Fast Fourier Transform. Nevertheless, a fine discretization of the orientation space gets rather costly in 3D. This is why regardless of the robustness of the anisotropic Gaussian filter method other methods are preferred for truely 3D fiber systems, e.g. [28,30,43], see the comparison in [32]. Due to the specific manufacturing process of fiber reinforced SMC and the samples being cut directly from the planar sheets, the fiber directions in the SMC samples considered here are however mostly localized within a plane. This layered structure of the samples justifies slice-wise 2D analysis here.

It is remarkable that the described method can be applied directly to the input gray value images, thus avoiding the error prone segmentation of individual fibers. In particular, this means, there is no need to separate crossing or touching fibers which requires ambiguous assignment of pixels to a certain fiber.

A binarization of the fiber system however helps to exclude not well-defined direction measurements from background pixels. This is achieved by deciding for each pixel whether it belongs to the fiber system or to the matrix. The decision is based on the filter responses since they provide a measure for the specificity of the local direction and thus are expected to be much stronger inside the fiber system than in the matrix. Niblack's locally adaptive thresholding method [44] applied to the image containing the maximal filter responses yields the desired binarization as shown in Fig. 4(b).

The thickness $2r$ of the elliptical filter mask governs the size of structures taken into account by the orientation analysis. Structures thinner than $2r$ will be smoothed and thus suppressed. Clearly, $2r$ should be chosen close to the thickness of the fiber bundles as they are emphasized that way. Nevertheless, a rough approximation of the thickness still ensures good orientation estimation since the Gaussian filter response will still be strong in fiber direction if enough edge information is preserved. The resulting principal direction of the fiber orientation distribution is robust w.r.t. slight changes of r. If however, r is chosen considerably too large, then too much edge information is removed and the resulting orientation distribution's variance increases.

Finally, boundary effects have to be suppressed to get a reliable result. For pixels with a distance to the image or sample boundary less than the longer axis of the filter mask, directions close to the direction of the boundary are preferred. Therefore, these pixels – referred to as border pixels in the following – have to be excluded from the analysis.

The preferred direction can be robustly identified without binarization of the fiber system and without suppressing the edge effects. The variance of the estimated orientation distribution increases however and the degree of anisotropy is underestimated accordingly. In the special application case considered here, these two factors influence the result much stronger than the thickness $2r$ as the fiber bundle thickness varies anyway. It is however important to choose the Niblack binarization parameters such that no false positive fiber pixels are detected. The edge length w of the sliding window was therefore chosen in the same range as the thickness parameter, that is $w = 4r$.

2.5. Orientation tensor and degree of anisotropy

Given the fiber system and the local fiber directions $v(x)$ with components $v_i, v_j, i,j = 1,\dots,d$, where d denotes the dimension of space, the averaged outer product of v_i, v_j yields the second order orientation tensor [45]

$$a_{ij} = \oint v_i\, v_j\, \rho(dv), \quad i,j = 1,\dots,d. \tag{3}$$

From the image data, an estimator $\widehat{a}$ of the component a_{ij} is derived by averaging the product $v_i(x)\, v_j(x)$ over a predefined sub-volume W in the form

$$\widehat{a}_{ij} = \frac{1}{\#(W \cap B)} \sum_{x \in (W \cap B)} v_i(x)\, v_j(x), \tag{4}$$

where B is the fiber system and $\#$ denotes the number of elements. The eigenvector corresponding to the largest eigenvalue $l_{\max}$ of the $d \times d$ matrix $(\widehat{a}_{ij})_{i,j=1,\dots,d}$ now yields the principal fiber direction m. If the fibers are isotropically distributed, then the eigenvalues of $(\widehat{a}_{ij})_{i,j=1,\dots,d}$ are the same. The more anisotropic the fiber direction distribution becomes, the stronger differ the maximal and the minimal eigenvalue, $l_{\max}$ and $l_{\min}$, respectively. Thus, a measure for the degree of anisotropy α, which allows for quantitative comparison of different material samples, can be derived from the ratio of these two values:

$$\alpha = 1 - \frac{l_{\min}}{l_{\max}}. \tag{5}$$

The degree of anisotropy in Eq. (5) thus assumes values between 0 and 1, where $\alpha = 0$ corresponds to an ideal isotropic fiber distribution. In the 2D case, $\alpha = 1$ corresponds to a system where all fibers are parallel to the principal fiber direction. In 3D, $\alpha = 1$ being equivalent to $l_{\min} = 0$ means that all fibers are oriented within a plane. The distribution of the orientations within this plane can however vary from being isotropic to being concentrated in one direction.

2.6. Fatigue tests

Subsequent to imaging and image analysis, the SMC samples have been investigated experimentally in order to reveal the influences of fiber orientation and fiber weight content on the fatigue strength behaviour.

The specimens were sinusoidally loaded under alternating constant amplitude loading (Fig. 3(b)). That is, the stress ratio R, defined as the ratio between minimum σ_u and maximum stress σ_o within one load cycle, was chosen to be R=-1. This choice was motivated by the final application scenario – a wheel. The tests were carried out on servo hydraulic test rigs as shown in Fig. 3(a) where the test load is transferred to the specimen by friction using manual clamping, under load control and at room temperature 23 °C. A support preventing buckling of the specimen during the compressive load half cycle but not affecting the load-dependent deformation was used, see Fig. 3 and [46] for details. Specimens, which had not failed after 5×10^6 load cycles, were considered run-out specimens and not used in the subsequent fatigue analysis.

3. Results and discussion

3.1. Image analytic orientation analysis

In the following we describe our findings in the application of the anisotropic Gaussian method for directional fiber analysis to SAM- and μ-CT-images of fiber reinforced SMC material samples. The fibers that can be seen on the micrographs actually represent whole fiber bundles, however, in the image analysis, for simplicity, they can be treated as single fibers. In the following, the word fiber is therefore used synonymous for fiber bundle. As described above, the fibers in the SMC are essentially oriented within a plane. That is, the direction distribution $\rho(A)$ defined in Eq. (1) is concentrated on the equator. Hence, in this case it is justified to consider the measure

$$\rho_0(A) = 2\,\rho(A) \tag{6}$$

on the space $(-90°, 90°]$ of non-oriented directions in the x-y-plane instead of $\rho(A)$ of Eq. (1) on the space S^2_+ of non-oriented directions in Euclidean space. The set $A \subset (-90°, 90°]$ in Eq. (6) is now a measurable set of non-oriented directions in the $x-y$-plane. Consequently, information about the direction distribution can be extracted from 2D images obtained by SAM or as slices of 3D μ-CT images. For our image analysis, a total of 180 directions,

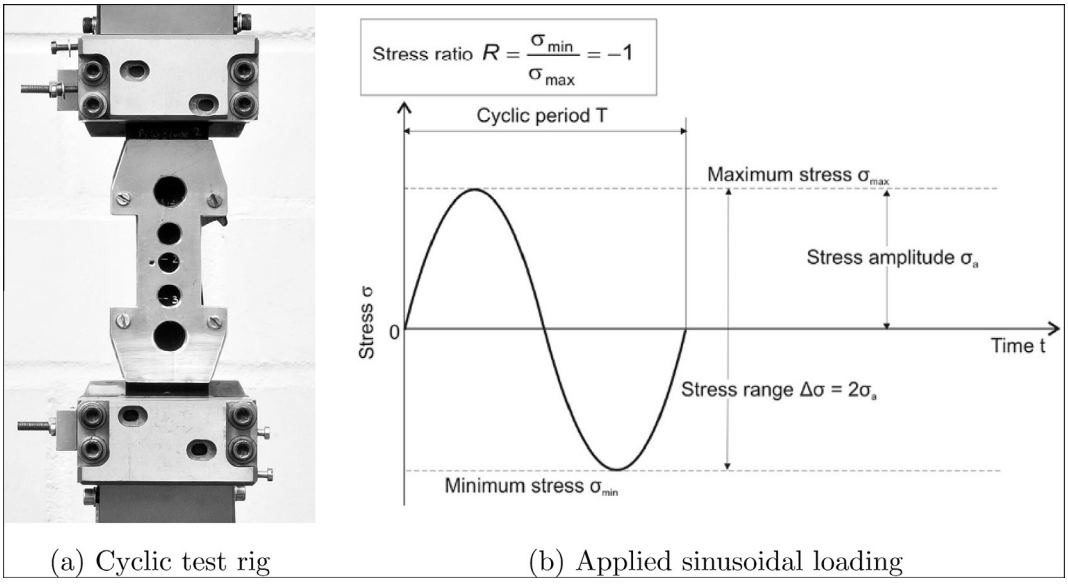

Fig. 3. Experimental setup for the fatigue tests. Cyclic test rig with test specimen and fitted buckling support and the applied sinusoidal loading with stress ratio R = −1. The specimen is mounted behind the visible buckling support whose holes serve for cooling the specimen.

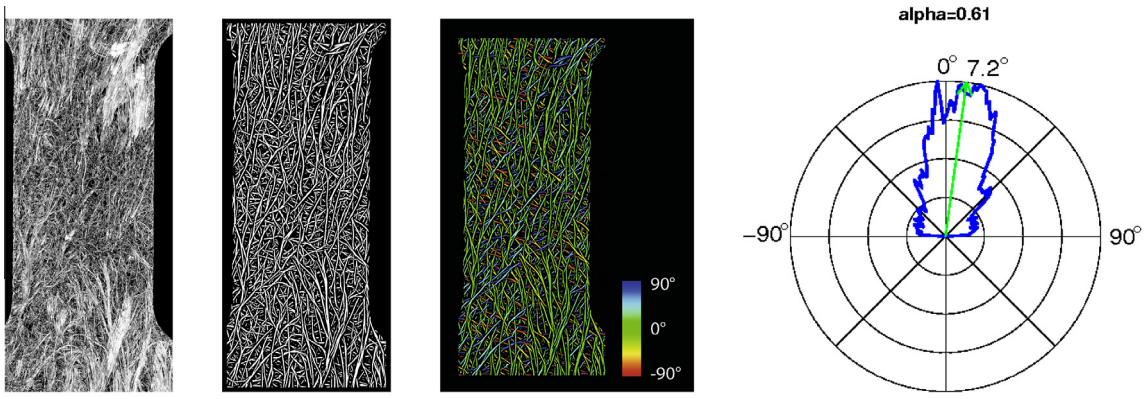

(a) original (b) fiber system (c) color coded orientations on fiber system (d) circular histogram

Fig. 4. Orientation analysis for a SAM image of an SMC sample with 30 wt% fibers. Original SAM gray value image with 1280 × 1024 pixels and 256 gray values, segmented fiber system (white) and matrix (black), and color-coded local directions, 0° = vertical, 90° = horizontal direction. Results are masked with the fiber system and border regions removed to avoid edge effects. The degree of anisotropy according to Eq. (5) is $\alpha = 0.61$. The principal fiber direction indicated by the green arrow is $m = 7.2°$.

evenly distributed in the interval $A \subset (-90°, 90°]$ are used throughout, resulting in a sufficient angular resolution while at the same time keeping the computational effort low, both for the processing steps and the analysis. The results for the SAM images and the μ-CT images are shown in Figs. 4 and 5. The orientation analysis results for CT and SAM image data turn out to agree very well measured by the deviation of principal direction as well as degree of anisotropy. See Fig. 5 for a comparison of just one layer and Fig. 6 for a comparison of several layers. However, for deeper layers, the SAM signal gets more and more diffuse due to structural information from higher layers being superimposed on the current one. More general, the principal direction is robust with respect to different processing while the degree of anisotropy reacts very sensitively. In particular masking with the fiber system as described above results in a considerable narrowing of the histogram since local directions measured with low reliability are suppressed. The observed degrees of anisotropy are mainly in the range $0.2 < \alpha < 0.7$ with a few outliers at $\alpha = 0.1$ and $\alpha = 0.9$.

3.2. Fatigue test results

In order to investigate the correlation of image analytic and mechanical testing results, we reconsider the samples from [46] that have been imaged by CT before testing.

The samples were assigned to three classes with respect to fiber orientation according to the image analytic results reported in Table 1. The classes are 0°, 45°, and 90°, where the angle is the one between measured preferred fiber orientation and load direction. That is, in the 0° specimens, the preferred fiber orientation is parallel to the load direction while for the 90° specimens, the fibers are oriented perpendicular to the load direction. All specimens feature a degree of anisotropy $\alpha > 0.5$.

Typical areas of fracture of the cyclically loaded flat specimens are shown in Fig. 7(a). The 90° specimens fractured perpendicular to the direction of force. For the 45° specimens, the fractures occurred diagonally to the direction of the force, i.e. parallel to the fibers. Hence, in both cases, the matrix failed and the fracture occurred along the pronounced orientation of the fibers. The 0° specimens fractured in an irregular pattern, as the fibers aligned parallel to the applied force determine the failure behaviour. These qualitative findings meet expectations [46]: The strain in the specimen is generated by matrix deformations and failure usually initiates at the weakest point within the stressed material volume. Hence, in heterogeneous materials like the glass fiber reinforced SMC, where stiff fibers reinforce a weak matrix, local failure occurs first in the matrix or at the fiber–matrix interface.

3.3. Correlation of image analytic and experimental results

Material behaviour in high-cycle fatigue domains is usually characterized by an S-N curve, also known as a Wöhler curve [46] – a graph of the cyclic stress amplitude a versus the number of cycles to failure, as shown in Fig. 7(b).

Fig. 7(b) shows the S-N curves for specimens with 20wt% fibers. The samples were assigned to the classes 0°, 45°, and 90° according to the image analytically measured fiber orientations reported in Table 1. The image analytically defined classes of specimen differ clearly with respect to fatigue strength as the order of the fitted S-N curves shows – highest strength at 0° fiber orientation to lowest strength at 90° fiber orientation.

Fig. 7 shows that the image analytically determined fiber orientation is well suited to predict local material behaviour.

The preferred fiber direction which was thus obtained via image analysis may now be used to align stress components with the material's coordinate systems. Next, we will show how to combine this result and a suitable failure hypothesis to derive failure envelopes for a given material.

In general, for a plane stress state, the collective of estimated critical multi-axial stress states may be displayed as failure envelope in a 3D stress space with the fatigue strengths in load direction σ_0° and orthogonal to it $\sigma_9 0^\circ$ and the shear strength τ in the plane as coordinate axes. A particular stress state may be visualized as vector and the application of the failure hypothesis may be interpreted as determination of the distance between the vector and the envelope. For fatigue life assessment, the original formulation needs to be modified by adopting fatigue strengths instead of static strengths at definition of the hypothesis. Then, each envelope represents the fatigue strengths at the specific failure number of cycles correlating to the uni-axial fatigue strengths at definition. The formula of the adapted Tsai-Wu failure hypothesis [47] for

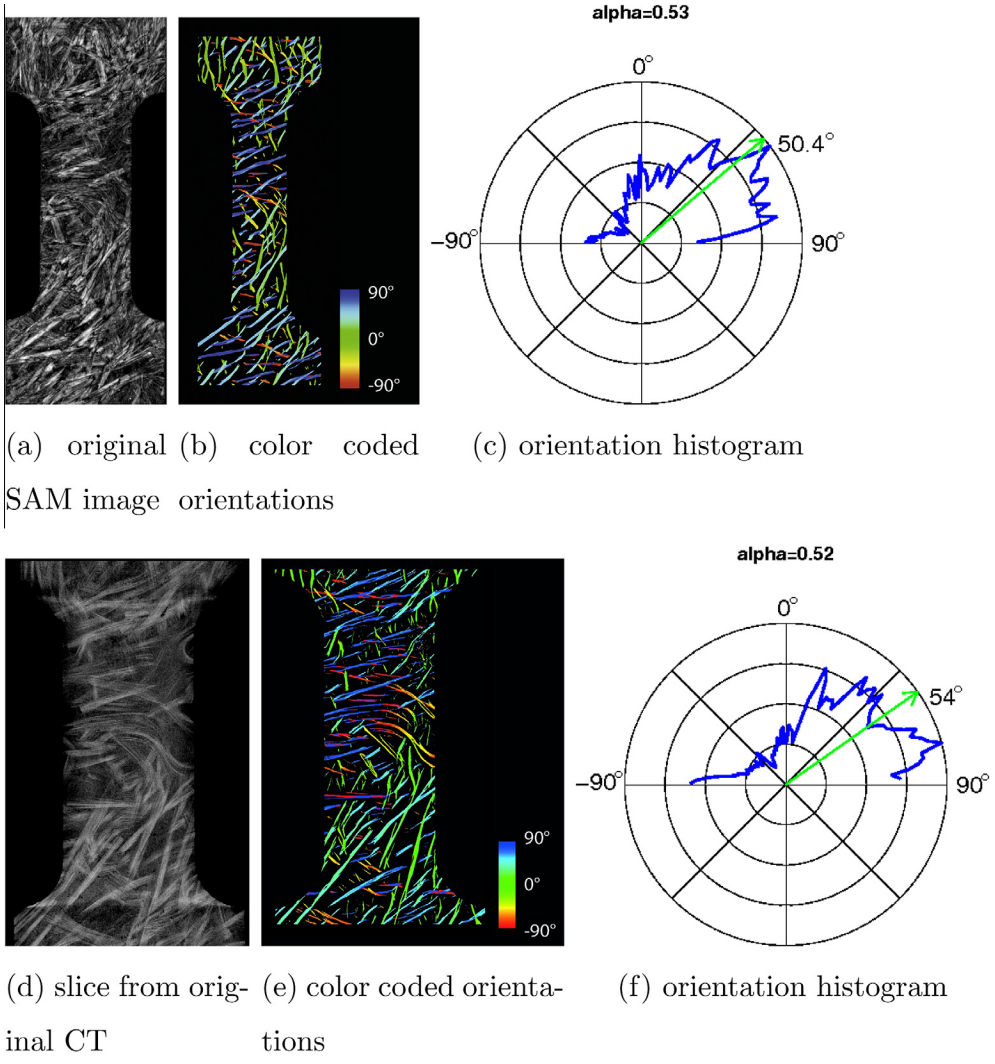

Fig. 5. Comparison of orientation analysis results based on SAM and 2D slice-wise analysis of μ-CT image data for a sample with 30 wt% fibers and main orientation 45°. The SAM image is focused on a depth of about 0.41 mm. The degree of anisotropy according to Eq. (5) is $\alpha = 0.53$. The principal fiber direction indicated by the green arrow is m = 50.4°. Slice No. 24 of the CT image at sample depth 0.41 mm is the one corresponding closest to the SAM image. The principal direction in slice No. 24 is $m = 54°$ and the degree of anisotropy $\alpha = 0.525$.

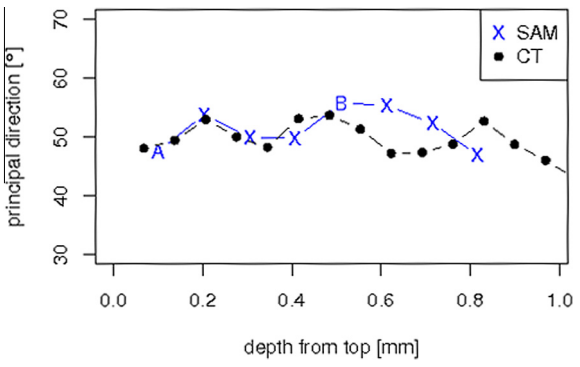

Fig. 6. Image analytically measured principal fiber bundle orientation based on SAM and computed tomography (CT) images for the sample from Figs. 2 and 5. Layers A and B are those shown in Fig. 2(a) and (b), respectively.

Table 1
Image analytically measured main fiber bundle orientation and degree of anisotropy for the fatigue testing samples from Fig. 7.

Sample	m	stddev(m)	α	stddev(α)
1	−2.1°	4.2°	0.664	0.035
2	0.3°	1.3°	0.646	0.029
3	−0.7°	2.6°	0.691	0.033
4	−4.7°	3.5°	0.643	0.042
5	−0.4°	3.4°	0.676	0.032
11	42.2°	0.8°	0.603	0.041
12	42.9°	1.5°	0.604	0.028
13	40.7°	3.2°	0.568	0.024
14	42.1°	1.6°	0.597	0.035
15	42.1°	1.6°	0.645	0.040
21	−89.8°	2.4°	0.566	0.045
22	−88.8°	1.8°	0.581	0.037
23	89.7°	3.1°	0.549	0.035
24	81.2°	3.5°	0.536	0.126
25	83.9°	3.6°	0.577	0.052

fatigue strength evaluation of a plane stress state for a transversally isotropic material has the following form [48]:

$$F_{11}\sigma_{0^\circ}^2 + 2F_{12}\sigma_{0^\circ}\sigma_{90^\circ} + F_{22}\sigma_{90^\circ}^2 + F_{66}\tau_{12}^2 + F_1\sigma_{0^\circ} + F_2\sigma_{90^\circ} \leq 1$$

with the following strength coefficients:

$$F_{11} = \frac{1}{XX'},\ F_1 = \frac{1}{X} - \frac{1}{X'},\ F_{22} = \frac{1}{YY'},\ F_2 = \frac{1}{Y} - \frac{1}{Y'},$$

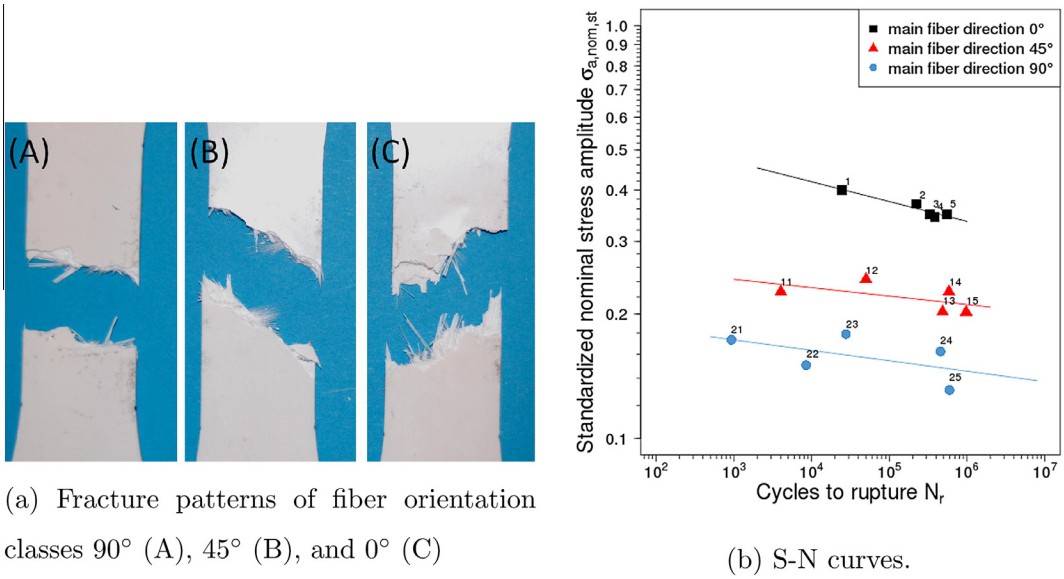

(a) Fracture patterns of fiber orientation classes 90° (A), 45° (B), and 0° (C)

(b) S-N curves.

Fig. 7. Correlation of macroscopic behaviour and fiber orientation classes (0°, 45°, and 90° relative to the loading direction) for SMC samples with 20 wt% fibers. Orientations result from image analytic measurements as described in Sections 2.4 and 2.5.

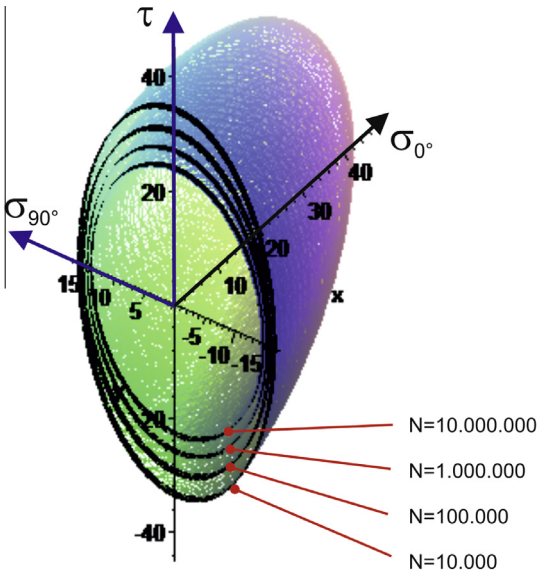

Fig. 8. Failure-envelopes for several numbers of cycles, based on the measured S-N curves and the failure hypothesis by Tsai and Wu [47]. The principal axes of the ellipsoids correspond to the fatigue strengths in main fiber direction σ_{0° and orthogonal to it σ_{90°. Stress in a certain direction, applied in N cycles yields the life time defined by the intersection point of the stress vector with the ellipsoid surface corresponding to N.

$$F_{12} = -\frac{1}{2}\sqrt{F_{11}F_{22}},\quad F_{66} = \frac{1}{S^2},$$

where $X = \sigma_x^{N,R} = X'$ denotes the fatigue strength in x-direction, here 0°, at N stress cycles at stress ratio R and $S = \tau_x^{N,R}$ is the shear fatigue strength at N stress cycles at stress ratio R. Correspondingly, Y denotes the fatigue strength in y-direction, here 90°.

Based on the measured S-N curves and on the failure hypothesis by Tsai and Wu [47], failure-envelopes for different numbers of cycles can be calculated, see Fig. 8. It should be noted, that in the case of (uni-axial or multi-axial) off-axis loading, the resulting stress components need to be transformed to the material coordinate system, which depends on the local fiber orientations, before application of this failure hypotheses. Also, it should be taken into account, that due to the anisotropy, off-axis loading causes additional coupled stress components. Thus knowing the strength related to the real fiber orientation is very important for a good component design. Hence, the local orientation of the fiber system has to be determined before adopting a failure hypothesis. Then, for example, the local stress vectors can be calculated in the local material coordinate system based on a given proportional loading of the component. The point, where the stress vector hits the failure envelope for the given number of cycles, finally represents the expected life time.

4. Conclusions

Knowledge of mechanical properties and structural durability assessment is essential for human safety in the lightweight design of safety-relevant components in aviation or car industry. In essence, the structural durability of a component is influenced mainly by the parameters loading, design (i.e. the shape), material, and manufacturing process. For an estimation of the service life of a component, the service loading and the fatigue strength have to be determined.

SMC is a randomly oriented long fiber reinforced composite. The resulting anisotropic behaviour of the material has to be taken into account when estimating the service life and identifying weaknesses of the design of components. More precisely, numerical simulation of macroscopic properties has to incorporate local microstructure characteristics like fiber orientation (degree of anisotropy and preferred orientation) and fiber weight content.

In this paper, quantitative image analysis has proved to deliver these essential microstructural data. Two non-destructive imaging techniques – SAM and μCT – combined with local fiber orientation estimation using anisotropic Gaussian filters, yield reliable robust results. The thus derived degree of anisotropy and preferred fiber direction are shown to correlate closely with material behaviour in fatigue experiments.

Modern imaging techniques and image analysis methods thus enable improved simulation of mechanical properties as local microstructural differences can be captured and incorporated into the simulation scheme.

Acknowledgement

This research was funded by the Fraunhofer-Gesellschaft zur Förderung der angewandten Forschung e. V., Germany, through grant 100129 (WISA Hochfeste Kunststoffe).

References

[1] Cornsweet TM. Advanced composite materials. Science 1970;168 (3930):433–8.
[2] Hogg PJ. Composites in armor. Science 2006;314(5802):1100–1.
[3] Tsai L, Prakash V, Rajendran AM, Dandrekar DP. Structure of shock waves in glass fiber reinforced polymer matrix composites. Appl Phys Lett 2007;90 (6):061909.
[4] Palmer J, Savage L, Ghita OR, Evans KE. Sheet moulding compound (SMC) from carbon fibre recyclate. Compos Part A Appl Sci Manuf 2010;41(9):1232–7.
[5] Le TH, Dumont PJJ, Orgéas L, Favier D, Salvo L, Boller E. X-ray phase contrast microtomography for the analysis of the fibrous microstructure of SMC composites. Compos Part A Appl Sci Manuf 2008;39(1):91–103.
[6] Thornton PH, Jeryan RA. Crash energy management in composite automotive structures. Int J Impact Eng 1988;7(2):167–80.
[7] Abrate S, Castanié B, Rajapakse YDS. Dynamic failure of composite and sandwich structures. Solid Mechanics and its Applications, vol. 192. Dordrecht: Springer; 2013.
[8] Brown KA, Brooks R, Warrior NA. The static and high strain rate behaviour of a commingled E-glass/polypropylene woven fabric composite. Compos Sci Technol 2010;70(2):272–83.
[9] Jendli Z, Fitoussi J, Meraghni F, Baptiste D. Anisotropic strain rate effects on the fibre-matrix interface decohesion in sheet moulding compound composites. Compos Sci Technol 2005;65(3–4):387–93.
[10] Fitoussi J, Meraghni F, Jendli Z, Hug G, Baptiste D. Experimental methodology for high strain-rates tensile behaviour analysis of polymer matrix composites. Compos Sci Technol 2005;65(14):2174–88.
[11] Hsiao HM, Daniel IM. Strain rate behavior of composite materials. Compos B 1998;29(5):521–33.
[12] Jacob GC, Starbuck JM, Fellers JF, Simunovic S, Boeman RG. Strain rate effects on the mechanical properties of polymer composite materials. J Appl Polym Sci 2004;94(1):296–301.
[13] Steinhauser MO. Computational multiscale modeling of fluids and solids – theory and applications. 1st Edition. Berlin, Heidelberg, New York: Springer; 2008.
[14] Jendli Z, Meraghni F, Fitoussi J, Baptiste D. Multi-scales modelling of dynamic behaviour for discontinuous fibre SMC composites. Compos Sci Technol 2009;69(1):97–103.
[15] Steinhauser MO, Grass K, Strassburger E, Blumen A. Impact failure of granular materials – Non-equilibrium multiscale simulations and high-speed experiments. Int J Plast 2008;25(1):161–82.
[16] Steinhauser MO. Computer simulation in physics and engineering. 1st ed. Berlin, Boston: deGruyter; 2013.
[17] Zhang D, Smith DE, Jack DA, Montgomery-Smith S. Numerical evaluation of single fiber motion for short-fiber-reinforced composite materials processing. J Manuf Sci Eng 2011;133(5):051002.
[18] Gonzales R, Woods R. Digital image processing. Prentice Hall; 2002.
[19] Ohser J, Schladitz K. 3D images of materials structures – processing and analysis. Weinheim: Wiley VCH; 2009.
[20] Stoyan D, Kendall WS, Mecke J. Stochastic geometry and its applications. 2nd ed. Chichester: Wiley; 1995.
[21] Fischer G, Eyerer P. Measuring spatial orientation of short fiber reinforced thermoplastics by image analysis. Polym Compos 1988;9(4):297–304.
[22] Bay RS, Tucker CL. Stereological measurement and error estimates for three-dimensional fiber orientation. Polym Eng Sci 1992;32(4):240–53.
[23] Jackson WC, Advani SG, Tucker CL. Predicting the orientation of short fibers in thin compression moldings. J Compos Mater 1986;20(6):539–57.
[24] Advani S, Tucker C. The use of tensors to describe and predict fibre orientation in short fiber composites. J Rheol 1987;31(8):751–84.
[25] Clarke A, Archenhold G, Davidson N. A novel technique for determining the 3D spatial distribution of glass fibres in polymer composites. Compos Sci Technol 1995;55(1):75–91.
[26] Eberhardt C, Clarke A. Fibre-orientation measurements in short-glass-fibre composites. Part I: automated, high-angular-resolution measurement by confocal microscopy. Compos Sci Technol 2001;61(10):1389–400.
[27] Sandau K, Ohser J. The chord length transform and the segmentation of crossing fibres. J Microsc 2007;226(1):43–53.
[28] Altendorf H, Jeulin D. 3d directional mathematical morphology for analysis of fiber orientations. Image Anal Stereol 2009;28(3):143–53.
[29] Viguié J, Latil P, Orgéas L, Dumont PJJ, Rolland du Roscoat S, Bloch J-F, Marulier C, Guiraud O. Finding fibres and their contacts within 3D images of disordered fibrous media. Compos Sci Technol 2013;89:202–10.
[30] Krause M, Hausherr J, Burgeth B, Herrmann C, Krenkel W. Determination of the fibre orientation in composites using the structure tensor and local X-ray transform. J Mater Sci 2010;45(4):888–96.
[31] Eberly D, Gardner R, Morse B, Pizer S, Scharlach C. Ridges for image analysis. J Math Imaging Vis 1994;4(4):353–73.
[32] Wirjadi O, Schladitz K, Easwaran P, Ohser J. The volume-weighted direction distribution in image analysis of fibre reinforced composites. Image Anal Stereol 2016. accepted for publication.
[33] Wirjadi O. Models and algorithms for image-based analysis of microstructures. Technische Universität Kaiserslautern; 2009. Ph.D. thesis.
[34] Lampert CH, Wirjadi O. An optimal non-orthogonal separation of the anisotropic Gaussian convolution filter. IEEE Trans Image Process 2006;15 (11):3501–13.
[35] Jeffery GB. The motion of ellipsoidal particles immersed in a viscous fluid. Proc R Soc London A: Math Phys Eng Sci 1922;102(715):161–79.
[36] Hennicke J, Netzelmann U, Shi Y. High-frequency ultrasound detection of small defects in si3n4 ceramic. Nondestr Testing Eval 1997;13(3): 139–47.
[37] Arnold W, Netzelmann U, Pangraz S. Characterization of surfaces by acoustic imaging techniques. In: Henry SD, editor. Friction, lubrication and wear technology, ASM Handbook 18. Materials Park, OH: ASM International Inc.; 1992. p. 406–13.
[38] Briggs A, Kolosov O. Acoustic microscopy. 2nd ed. Oxford University Press; 2009.
[39] Kalender W, Seissler W, Klotz E, Vock P. Spiral volumetric ct with single breath-hold technique, continuous transport, and continuous scanner rotation. Radiology 1990;176:181–3.
[40] Kasperl S, Vontobel P. Application of an iterative artefact reduction method to neutron tomography. Nuclear Instrum Methods Phys A 2005;542 (13):392–8.
[41] Kiderlen M. Estimating the Euler characteristic of a planar set from a digital image. J Vis Commun Image R 2006;17:1237–55.
[42] Altendorf H. 3d morpohological analysis and modeling of random fiber networks. TU Kaiserslautern, MINES ParisTech; 2011. Ph.D. thesis.
[43] Redenbach C, Rack A, Schladitz K, Wirjadi O, Godehardt M. Beyond imaging: on the quantitative analysis of tomographic volume data. Int J Mater Res 2012;2:217–27.
[44] Niblack W. An introduction to digital image processing. New York: Prentice-Hall; 1986.
[45] Tucker C, Advani S. Processing short-fiber systems. In: Advani S, editor. Flow and Rheology in Polymer Composites Manufacturing, Composite Materials. Amsterdam, NL: Elsevier; 1994. p. 147–202.
[46] Fleckenstein J, Jaschek K, Büter A, Stoess N. Fatigue design optimization of safety components made of SMC. 11TH International Congress on the Mechanical Behaviour of Materials, Como, Italy.
[47] Tsai SW, Wu EM. A general theory of strength for anisotropic materials. J Compos Mater 1971;5(1):58–80.
[48] Moosbrugger E, DeMonte M, Jaschek K, Fleckenstein J, Büter A. Multiaxial fatigue behaviour of a short-fibre reinforced polyamide experiments and calculations. Materialwiss Werkstk 2011;42(10):950–7.